Spectrochimica Acta Part A: Molecular and Biomolecular Spectroscopy 131 (2014) 388–397

Contents lists available at ScienceDirect

Spectrochimica Acta Part A: Molecular and Biomolecular Spectroscopy

journal homepage: www.elsevier.com/locate/saa

DFT calculations, spectroscopic, thermal analysis and biological activity of Sm(III) and Tb(III) complexes with 2-aminobenzoic and 2-amino-5-chloro-benzoic acids

Amr A. Essawy [a], Manal A. Afifi [a], H. Moustafa [b,*], S.M. El-Medani [a]

[a] Chemistry Department, Faculty of Science, Fayoum University, 63514 Fayoum, Egypt
[b] Chemistry Department, Faculty of Science, Cairo University, Giza, Egypt

HIGHLIGHTS

- ($Sm[C_7H_6NO_2]_3$, $Tb[C_7H_6NO_2]_3$, $Sm[C_7H_5NO_2Cl]_3$ and $Tb[C_7H_5NO_2Cl]$,) complexes are prepared.
- Elemental, IR, UV, mass spectra and thermal analyses.
- An octahedral geometry has been assigned for the prepared $M(AA)_3$ complexes.
- Biological activities against gram positive, gram negative bacteria and fungi.
- Optimized geometry calculations at the B3LYP/6-311++G** level of theory.

GRAPHICAL ABSTRACT

The optimized geometry of the $Sm(AA)_3$ complex.

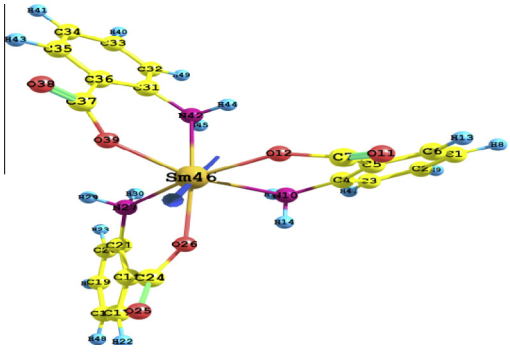

ARTICLE INFO

Article history:
Received 29 January 2014
Received in revised form 16 March 2014
Accepted 14 April 2014
Available online 30 April 2014

Keywords:
Anthranilic acid
Chloroanthranilic acid
Lanthanide complexes
Spectral studies
DFT calculation
Biological activity

ABSTRACT

The complexes of Sm(III) and Tb(III) with 2-aminobenzoic acid (*anthranilic acid*, AA) and 2-amino-5-chlorobenzoic acid (*5-chloroanthranilic acid,* AACl) were synthesized and characterized based on elemental analysis, IR and mass spectroscopy. The data are in accordance with 1:3 [Metal]:[Ligand] ratio. On the basis of the IR analysis, it was found that the metals were coordinated to bidentate anthranilic acid via the ionised oxygen of the carboxylate group and to the nitrogen of amino group. While in 5-chloroanthranilic acid, the metals were coordinated oxidatively to the bidentate carboxylate group without bonding to amino group; accordingly, a chlorine-affected coordination and reactivity-diversity was emphasized. Thermal analyses (TGA) and biological activity of the complexes were also investigated. Density Functional Theory (DFT) calculations at the B3LYP/6-311++G (d,p)_ level of theory have been carried out to investigate the equilibrium geometry of the ligand. The optimized geometry parameters of the complexes were evaluated using SDDALL basis set. Moreover, total energy, energy of HOMO and LUMO and Mullikan atomic charges were calculated. In addition, dipole moment and orientation have been performed and discussed.

Introduction

Anthranilic acid is biosynthesized from chorismic acid. It plays a vital part in the biosynthesis of tryptophan and its derivatives via

* Corresponding author. Tel.: +20 1002589404; fax: +20 2 35676576.
E-mail address: hmamoustafa@yahoo.com (H. Moustafa).

http://dx.doi.org/10.1016/j.saa.2014.04.134
1386-1425/

the attachment of phosphoribosyl pyrophosphate to the amine group, as well as in several types of alkaloids [1]. Anthranilic acid is a versatile and low cost starting material in organic synthesis to generate the benzyne intermediate and to synthesize benzo-fused heterocycles [1]. Industrially, anthranilic acid is used as an intermediate for production of dyes, pigments, and saccharin. It and its esters are used in preparing perfumes to imitate jasmine and orange, pharmaceuticals and UV-absorber as well as corrosion inhibitors for metals and mold inhibitors in soya sauce.

In addition, anthranilic acid could be commonly used as fluorescent tag in detection of monosaccharides using liquid chromatography or capillary electrophoresis. It provides a monosaccharide labeling with a highly reproducible and accurate results [2]. Recently, a series of N-benzoyl anthranilic acid derivatives were prepared as inhibitors of penicillin binding proteins [3]. Other literatures [4,5] showed that substitution of the amino group in AA by different substituted aryl or heteroaryl moieties could markedly modulate the anti-inflammatory activity. The compound N-phenylanthranilic acid is used as a common intermediate in the synthesis of pharmaceutically important molecules such as antimalarials and antineoplatics [6].

Fluorescent rare earth complexes are of great interest owing to their broad applications in biochemistry, material chemistry, medicine and so forth. Rare earth complexes with carboxylic acids may be used as structural and functional probes of biological macromolecule systems [7]. It was found that the complex of a reactive ternary Tb(III) could be excited by 365 nm ultraviolet, and emitted green light attributed to the characteristic emission of Tb(III) ion [8].

Investigation of coordination compounds of samarium and terbium ions with organic ligands has been attracted significant attentions that focus on several potential applications of its luminescence [9–11]. Such as application in the lighting industry, ability to provide electroluminescent material for organic light emitting diodes (OLEDs) [12] and optical fibers for telecommunications, a capacity to yield functional complexes for biological assays and medical imaging purposes [13–15].

Anthranilic acid offers two possible coordination sites, one carboxylic and one amino group. The coordination of metal ions toward the ligand is discussed very controversial in the literature. For example, a bidentate binding mode via the two oxygen atoms of the carboxylic group was postulated for Tb(III) anthranilate complexes in solid state [16,17]. Other authors suggested that the coordination of the metal ion takes place via a chelate formation through the nitrogen atom of the amino group and one oxygen atom of the carboxylic group [18,19].

Large discrepancies have been published for the interaction of anthranilic acid with trivalent lanthanides [20]. By employing an alternative synthetic route, a range of lanthanoid anthranilates were synthesized and characterized. The results reveal a diverse range of structural classes exhibited by lanthanoid anthranilates [21]. This prompted us to confirm the pattern of coordination in these complexes using for the first time a dual experimental and theoretical insight. Sm(III) and Tb(III) anthranilate and 5-chloroanthranilate solid complexes were synthesized then spectroscopically characterized and subjected to extensive theoretical calculations. The DFT calculations for the model systems correlate well with experimentally determined metrical parameters. Moreover, the thermal stability of the reported metal complexes as well as their biological activities has been studied.

Experimental

Materials and reagents

All chemicals and reagents were of reagent grade quality and were used as received without further purification. Anthranilic acid, (2-amino benzoic acid, AA) and chloroanthranilic acid (2-amino-5-chloro benzoic acid, AACl) were provided from Fluka. Terbium chloride hexahydrate, $TbCl_3{\cdot}6H_2O$ was obtained by treating Tb_4O_7 (99.9%, Chempur) with concentrated HCl and the surplus HCl was removed by evaporation. The residue was dissolved with deionized water and evaporated for three times results finally to the crystals of hexahydrate terbium chloride. Samarium chloride hexahydrate, $SmCl_3{\cdot}6H_2O$ (99.9%) was provided from Sigma–Aldrich. Bi-distilled water is usually used in all preparations.

Instrumentation

Elemental microanalyses of the separated solid chelates for C, H, N were performed in the Microanalytical Center at Cairo University. The analyses were repeated twice to check the accuracy of the data. Infrared spectra were recorded on a Perkin–Elmer FTIR type 1650 spectrophotometer in the region 4000–400 cm^{-1} as KBr discs. The absorption spectra were recorded with a double beam Perkin–Elmer Lambda 25 UV–Visible spectrophotometer. The pH was measured using pHs-JAN-WAY 3330 research pH meter at 25 °C. The thermal analysis (TG and DTA) were carried out in dynamic nitrogen atmosphere (20 mL min^{-1}) with a heating rate of 10 °C min^{-1} using Shimadzu TG-60H and DTA-60H thermal analyzers.

Synthesis of metal complexes

As an example, the anthranilate complex with Tb^{3+} ions was simply prepared by adding (126 mg) sodium bicarbonate of pure grade (Aldrich) to a hot water–ethanol solution (30 mL, 10:20 v/v) of an equimolar amount of AA (206 mg). The mixture was stirred for 15 min at 70 °C. After that, ethanolic solution (10 mL) of $TbCl_3{\cdot}6H_2O$ (186.69 mg, 0.5 mmol) was added drop wisely under continuous stirring. The resulting mixture was kept under stirring for 4 h at 60 °C forming a white precipitate. The precipitate was separated by filtration and washed with bidistilled water to separate sodium chloride from the solid formed complex which is insoluble in water. The complex dissolves readily in DMF, DMSO and in hot absolute ethanol. The complex was recrystallized from ethanol to give 231 mg of pure compound (Yield 81.6%). The same procedure was performed to synthesize the samarium anthranilate complex (Yield 80.3%) and in the synthesis of both samarium and terbium chloroanthranilate complexes giving yields of 85.7% and 84.8%, respectively.

Biological activity

The in vitro antimicrobial activity of the free ligand and their complexes were tested against the bacteria: *Staphylococcus aureus* (gram +ve) and Escherichia coli (gram −ve) in Mueller Hinton-Agar medium and fungi: *Aspergillus flavus* and *Aspergillus niger* in YPD-agar medium. The standard disc-agar diffusion method [22] was followed to determine the antibacterial and antifungal activity of the synthesized compounds. The tested compounds were dissolved in DMF (which has no inhibition activity), to get concentrations of 100 mg/mL. Uniform size filter paper disks (3 disks per compound) were impregnated by equal volume (0.1 mL) from the specific concentration of dissolved tested compounds and carefully placed on incubated agar surface. After incubation for 48 h at 37 °C, inhibition of the organisms which evidenced by clear zone surround each disk was measured and used to calculate the mean of inhibition zones [21,23].

Table 1
Elemental analysis and mass spectrometry data for AA and AACl lanthanide complexes.

Complex	C% Found (Calc.)	H% Found (Calc.)	N% Found (Calc.)	Mass spectrometry	
				M. Wt	*m/z*
$Sm(AA)_3$; $Sm[C_7H_6NO_2]_3$	44.7 (45.1)	3.3 (3.2)	7.7 (7.5)	558.76	543[p-O]$^+$
$Tb(AA)_3$; $Tb[C_7H_6NO_2]_3$	43.9 (44.5)	3.2 (3.2)	7.4 (7.4)	567.32	568[p]$^+$
$Sm(AACl)_3$; $Sm[C_7H_5NO_2Cl]_3$	36.8 (37.9)	2.4 (2.7)	6.4 (6.3)	662.23	663[P]+
$Tb(AACl)_3$; $Tb[C_7H_5NO_2Cl]_3$	38.5 (37.9)	2.5 (2.7)	6.3 (6.2)	670.80	671[p]$^+$

Computational method

Calculations have been performed using Khon–Sham's DFT method subjected to the gradient-corrected hybrid density functional B3LYP [24]. This function is a combination of the Becke's three parameters non-local exchange potential with the non-local correlation functional of Lee et al. For each structure, a full geometry optimization was performed using this function [25] and the 6-31G* bases set [26] as implemented by Gaussian 09 package [27]. No symmetry constrains were applied during the geometry optimization.

Results and discussion

Elemental analysis

The results of elemental analyses and mass spectrometry of the reported complexes are in good agreement with those required by the proposed molecular formulae (Table 1). It is clear from these data that the complexes are formed in 1:3 [Metal]:[Ligand] ratio. Mass spectra of the complexes $Sm(AA)_3$, $Tb(AA)_3$, $Sm(AACl)_3$ and $Tb(AACl)_3$ displayed molecular ion peaks at $m/z = 543$, 568, 663, and 671, respectively. The molecular ion peak at 543 corresponds to the parent molecular ion peak [p-O]$^+$, whereas the remainder ion peaks were referred to the molecular ion peak [p]$^+$. The molecular formulae of the complexes; $Sm(AA)_3$, $Tb(AA)_3$, $Sm(AACl)_3$ and $Tb(AACl)_3$ were found as $Sm[C_7H_6NO_2]_3$, $Tb[C_7H_6NO_2]_3$, $Sm[C_7H_5NO_2Cl]_3$ and $Tb[C_7H_5NO_2Cl]$, respectively.

IR spectroscopy

In order to study the types of bonding between the ligands and metal ions and to elucidate the structure of the obtained complexes, their IR spectra were recorded. The IR data of AA and AACl and their samarium and terbium complexes are listed in Table 2. The IR spectra of the complexes are compared with those of the free ligands in order to determine the coordination sites that may be involved in chelation. The carboxylic and amine groups are the possible bonding sites in the anthranilic acid with lanthanides.

The IR spectrum of anthranilic acid (AA) displayed two strong bands at 3324 and 3240 cm^{-1} due to $\nu_{as}(NH_2)$ and $\nu_s(NH_2)$ stretching frequencies, respectively, while the absorption band resulting from the deformation δNH_2 was found at 1618 cm^{-1} [28]. Furthermore, two important stretching vibrations were observed at 1664 and 1291 cm^{-1}. The band at 1664 cm^{-1} was attributed to the C═O stretching vibration of the carboxyl group and that occurred at 1291 cm^{-1} could be ascribed to the C—N stretching vibration [29]. Also, the IR spectrum of (AA) displayed two medium stretching bands at 1585 and 1420 cm^{-1} which corresponded to the asymmetric and symmetric stretching vibration of the carboxylate group ($\nu_{as}COO^-$ and ν_sCOO^-), respectively [28,30].

Similarly, the IR spectrum of the 5-chloroanthralinic acid (AACl) showed two strong bands at 3466 and 3356 cm^{-1} due to $\nu_{as}(NH_2)$ and $\nu_s(NH_2)$ stretching frequencies, respectively. The two bands at 1595 and 1237 cm^{-1} corresponded to the deformation δNH_2 vibration and the ν(C—N) stretching vibration, respectively. Furthermore, the IR spectrum showed a band at 1671 cm^{-1} corresponded to ν (C═O) and two bands at 1588 and 1483 cm^{-1} referred to $\nu_{as}COO^-$ and ν_sCOO^- stretching frequencies, respectively. In the IR spectra of the reported complexes, the bands corresponding to the C═O vibrations at 1664 and 1671 cm^{-1} (Table 2) disappeared entirely as reported in literature [28].

o-Anthranilate lanthanide complexes

The IR spectrum of the complex $Sm(AA)_3$ displayed stretching bands at 3475 and 3424 cm^{-1} due to $\nu_{as}(NH_2)$ and $\nu_s(NH_2)$ vibrations, respectively. Also, the complex $Tb(AA)_3$ showed two stretching bands at 3486 and 3363 cm^{-1} referred to $\nu_{as}(NH_2)$ and $\nu_s(NH_2)$ vibrations, respectively. These values showed significant frequency shifts with respect to the corresponding values of the free ligands. The shift values range from 123 to 184 cm^{-1}, (Table 2). The relatively high shift values $\Delta\nu_{as}(NH_2)$ and $\Delta\nu_s(NH_2)$ may indicate the coordination of Sm(III) and Tb(III) to *o*-anthranilic acid via the amine group (NH_2) [31]. This type of bonding could be ascertained by the lower frequency shift in the νC—N vibration by 39 and 34 cm^{-1} in the IR spectra of the two complexes $Sm(AA)_3$ and $Tb(AA)_3$, respectively. In addition, the appearance of ν(M—N) stretching bands at 425 for $Sm(AA)_3$ and at 448 cm^{-1} for $Tb(AA)_3$ confirmed the coordination of Sm(III) and Tb(III) to AA via the amine group (NH_2).

The carboxylic group is the second group participating in the bond of the anthranilic acid with lanthanides. Just as in the spectra of anthranilates of d-electron elements, the bands of asymmetric and symmetric vibrations of the COO^- group in the spectra of samarium and terbium anthranilates are displaced to lower frequencies [32]. The peaks due to $\nu_{as}COO^-$ of the two complexes $Sm(AA)_3$ and $Tb(AA)_3$ were shifted to lower frequencies by 68 and 63 cm^{-1} and the lower shifts in ν_sCOO^- were found to be 20 and 18 cm^{-1}, respectively (Table 2). The shifts in the asymmetric and symmetric stretching frequencies of the COO^- species in the

Table 2
Important IR data for AA and AACl and their Sm(III) and Tb(III) complexes.

Compound	[a]IR cm^{-1}												
	ν(C═O)	$\nu_{as}(NH_2)$	$\Delta\nu_{as}$ (NH_2)	$\nu_s(NH_2)$	$\Delta\nu_s(NH_2)$	ν(C—N)	ν_{as} COO^-	Δ ν_{as} COO^-	ν_s COO^-	$\Delta\nu_s$ COO^-	$(\nu_{as}\text{-}\nu_s)$ COO^-	ν(M—O)	ν(M—N)
(AA)	1664(m)	3324(s)	–	3240(s)	–	1291(m)	1585(b, m)	–	1420(m)	–	+165	–	–
$Sm(AA)_3$	–	3475(m)	+155	3424(m)	+184	1252(m)	1517(s)	−68	1400(s)	−20	+117	528(w)	425(w)
$Tb(AA)_3$	–	3486(m)	+162	3363(m)	+123	1257(m)	1522(s)	−63	1402(s)	−18	+120	527(w)	448(w)
(AACl)	1671(s)	3466(s)	–	3356(s)	–	1237(s)	1588(s)	–	1483(s)	–	+105	–	–
$Sm(AACl)_3$	–	3479(m)	+13	3365(m)	+9	1245(m)	1510(s)	−78	1427(m)	−56	+83	570(w)	–
$Tb(AACl)_3$	–	3481(m)	+15	3369(m)	+13	1245(m)	1510(s)	−78	1427(s)	−56	+83	572(w)	–

[a] s, strong; m, medium; w, weak; b, broad.

IR spectra of lanthanide complexes indicate that *o*-anthranilate is coordinated to Sm(III) and Tb(III) via the oxygen of the carboxylate group. This is confirmed by the appearance of new νM—O stretching bands at 528 and 527 cm^{-1} for Sm(III) and Tb(III) complexes, respectively.

5-Chloroanthranilate lanthanide complexes

The IR spectra of the complexes $Sm(AACl)_3$ and $Tb(AACl)_3$ displayed stretching medium bands at 3479 and 3481 cm^{-1} due to $\nu_{as}(NH_2)$ and at 3365 and 3369 cm^{-1} due to $\nu_s(NH_2)$ with lower shifts with respect to those of the free ligands (Table 2). The relatively small shift values of $\Delta\nu_{as}(NH_2)$ and $\Delta\nu_s(NH_2)$ may indicate that the amine group (NH_2) in the chloroanthranilate may not participate in the coordination to Sm(III) and Tb(III) in their chloroanthranalate complexes. This could be ascertained from the absence of ν(M—N) stretching band in the IR spectra of the two complexes $Sm(AACl)_3$ and $Tb(AACl)_3$. Comparing the $\Delta\nu_{as}(NH_2)$ and $\Delta\nu_s(NH_2)$ values of the anthranilate and the chloroanthranilate Sm(III) and Tb(III) complexes, revealed that the shift values for the anthranilate complexes (123–184 cm^{-1}) are higher than the corresponding values of the chloroanthranilate complexes (9–15 cm^{-1}). This indicates the participation of the anthranilate NH_2 group in the coordination to samarium and terbium while in chloroanthranilate complexes; chlorine atom greatly dimensioned the contribution of this coordination site.

The carboxylate group can participate in bonding of the 5-chloroanthranilate with lanthanides. On complexation, the $\nu_{as}COO^-$ and ν_sCOO^- bands in samarium and terbium complexes showed lower shifts by 78 and 56 cm^{-1}, respectively, with respect to the corresponding species in the ligands. The shift values of the bands to lower frequency indicate the degree of bond covalency. The lower shift of the peak $\nu_{as}COO^-$ (1585 cm^{-1}) was found to be 40–50 cm^{-1} for Cd, Ni, Co, Zn, Cu anthranilates [33]. Whereas in Sm (III) and Tb (III) anthranilate and 5-chloroanthranilate complexes; the shift values were found to be 63–78 cm^{-1}. The relatively higher shifts in the antisymmetric and symmetric stretching frequencies of the COO^- species in the IR spectra of the 5-chloroanthranilate complexes may indicate the coordination of the ligand to Sm(III) and Tb(III) via the two carboxylate oxygen atoms forming four membered ring. This is confirmed by the appearance of new νM—O stretching band at 570 and 572 cm^{-1} in the IR spectra of Sm(III) and Tb(III) complexes, respectively.

According to elemental analysis data and interpretation of IR spectra, samarium (III) and terbium (III) ions were expected to be coordinated to the *o*-anthranilate ion through a nitrogen atom of NH_2 group and oxygen of the carboxylate group [34], forming six membered ring in each complex, $Sm(AA)_3$ or $Tb(AA)_3$. On the other hand, Sm(III) and Tb(III) ions were bonded to the 5-chloroanthranilate ions through the two oxygen of the carboxylate ion forming four membered ring in $Sm(AACl)_3$ or $Tb(AACl)_3$ complex. The proposed structures of the reported complexes are shown in Scheme 1.

Thermogravimetric analysis

Thermogravimetry provides more insight into the composition and structure of the complexes. Thermal studies could be carried out using thermogravimetry (TG) and (DTG) techniques. Thermal

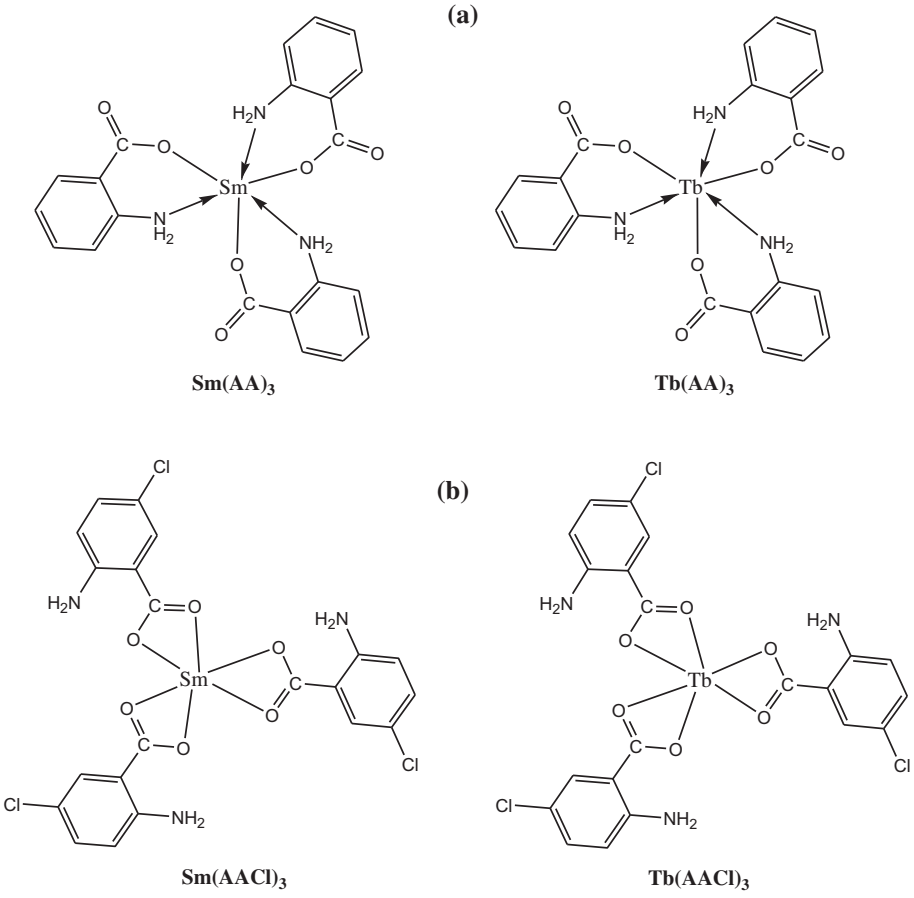

Scheme 1. The proposed structures of: (a) samarium and terbium anthranilate complexes and (b) chloroanthranilate complexes.

Table 3
Thermal analysis data for samarium and terbium complexes.

Complex	Decomposition step, K	DTG max, K	[a]*n*	Weight loss%	Mol. wt Found (Calc.)	Species eliminated	Solid residue Found, (calc.) %
$Sm(AA)_3$ $Sm[C_{21}H_{18}N_3O_6]$	330–637	598	1	10.04	56.10 (56.08)	C_3H_6N	29.82 (29.78)
	637–726	671	1	35.82	200.15 (200.17)	$C_{11}H_6NO_3$	SmO
	726–923	735, 875	2	24.32	135.89 (136.13)	$C_7H_6NO_2$	
$Sm(AACl)_3$ $Sm[C_{21}H_{15}N_3O_6Cl_3]$	563–626	605	1	9.87	65.36 (65.57)	$C_2H_6 + ½\ Cl_2$	34.40 (34.19)
	626–774	719	1	49.98	331.01 (331.17)	$C_{11}H_6N_3 + Cl_2 + 5/2\ O_2$	SmO + 5C
	774–936	825	1	5.93	39.27 (39.06)	C_3H_3	
$Tb(AA)_3$ $Tb[C_{21}H_{18}N_3O_6]$	423–700	674	1	63.72	361.47 (364.36)	$C_{20}H_{18}N_3 + 2\ O_2$	36.28 (35.76) $TbO_2 + C$
$Tb(AACl)_3$ $Tb[C_{21}H_{15}N_3O_6Cl_3]$	321–520	403	1	5.20	34.90 (35.5)	$½\ Cl_2$	35.31 (35.62)
	520–1074	746	1	59.49	399.00 (396.31)	$C_{17}H_{15}N_3 + 2O_2 + Cl_2$	$TbO_2 + 4C$

[a] *n* = Number of decomposition steps.

analysis is used to: (i) get information about the thermal stability of the metal complexes, (ii) suggest the presence of crystalline and hydrated water molecules and (iii) suggest a general scheme for thermal decomposition of the complexes. The results of thermal decomposition of the metal complexes indicated the absence of any type of water molecules as shown in Table 3.

Thermogravimetric analysis of $Sm(AA)_3$ and $Tb(AA)_3$ complexes

The TG plot of $Sm(AA)_3$, $Sm[C_{21}H_{18}N_3O_6]$, complex displayed four decomposition steps. Since the third and fourth decomposition steps were confused, three resolved and well-defined decomposition steps could be considered. The first decomposition step occurred in the temperature range 330–637 K with a net weight loss of 10.04% corresponding to elimination of (C_3H_6N) species (10.04% cal). The second decomposition peak occurred in the temperature range 637–726 K with a weight loss of 35.82% and corresponded to the material decomposition ($C_{11}H_6NO_3$) moieties (35.82% cal). The third decomposition step occurred in the temperature range 726–923 K with a weight loss of 24.32% corresponding to the elimination of ($C_9H_4N_2$) species (24.36% cal) to give finally the residue SmO (29.82%).

Thermal studies of the complex $Tb(AA)_3$, $Tb[C_{21}H_{18}N_3O_6]$, were carried out using thermogravimetry (TG) and (DTG) techniques. The TG plot of the complex showed one decomposition step in the temperature range 423–700 K giving a net weight loss of 63.72% corresponding to elimination of ($C_{20}H_{18}N_3 + 2O_2$) species (64.22% cal) to give finally the residue ($TbO_2 + C$) with 36.28%.

Thermogravimetric analysis of $Sm(AACl)_3$ and $Tb(AACl)_3$ complexes

The TG plot of $Sm(AACl)_3$, $Sm[C_{21}H_{15}N_3O_6Cl_3]$, complex displayed three resolved and well-defined decomposition steps. The first decomposition step occurred in the temperature range 563–626 K with a net weight loss of 9.87% corresponding to elimination of ($C_2H_6 + ½Cl_2$) species (9.90% cal). The second decomposition peak occurred in the temperature range 626–774 K with a weight loss of 49.98% and corresponded to the material decomposition ($C_{11}H_6N_3 + Cl_2 + 5/2O_2$) moieties (50.01% cal). The third decomposition step occurred in the temperature range 774–936 K with a weight loss of 5.93% corresponding to the elimination of (C_3H_3) species (5.90% cal) to give finally the residue (SmO + 5C) species (34.40%).

The TG plot of $Tb(AACl)_3$, $Tb[C_{21}H_{15}N_3O_6Cl_3]$, complex displayed two resolved and well-defined decomposition steps. The first decomposition step occurred in the temperature range 321–520 K with a net weight loss of 5.20% corresponding to elimination of $½Cl_2$ species (5.29% cal). The second decomposition peak occurred in the temperature range 520–1074 K with a weight loss of 59.49% and corresponded to the material decomposition ($C_{17}H_{15}N_3 + Cl_2 + 2O_2$) moieties (59.08% cal) to give finally the residue ($TbO_2 + 4C$) species (35.31%).

The sum of the eliminated and solid residual species for all lanthanide complexes confirmed their molecular formulae (Table 3).

Absorption spectra

The UV absorption spectra of 1×10^{-5} mol. L^{-1} ethanolic solution of AA, AACl and their tris-samarium and terbium complexes are presented in Fig. 1. Fig. 1A reveals a broad UV absorption band at λ_{max} = 331 nm with ε value around 21780 mol.$^{-1}$ L cm^{-1}. This band could be assigned to π–π^* transition in AA (spectrum 1).

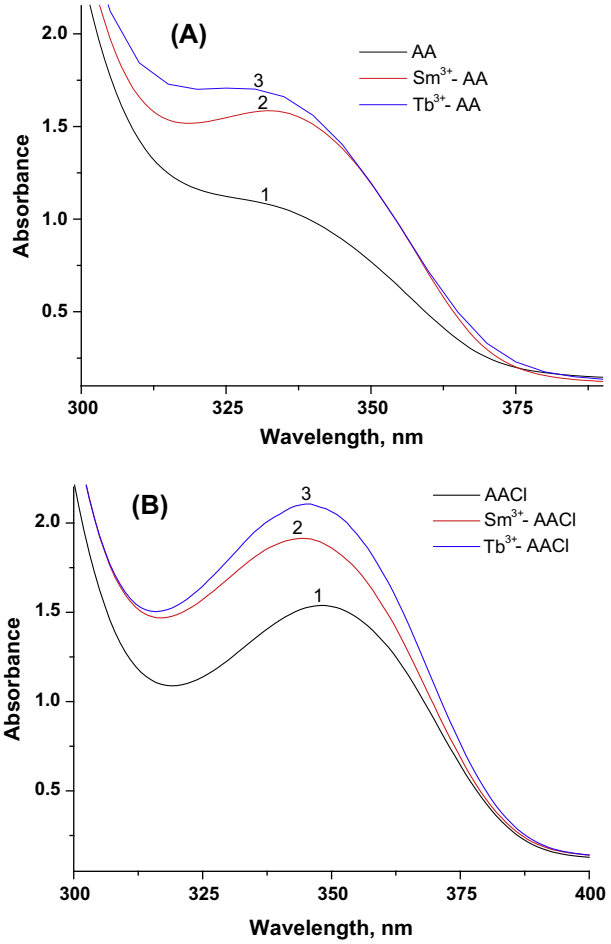

Fig. 1. (a) UV absorption spectra of AA (spectrum 1), Sm^{3+}-$(AA)_3$ (spectrum 2) and Tb^{3+}-$(AA)_3$ (spectrum 3). (b) UV absorption spectra of AACl (spectrum 1), Sm^{3+}-$(AACl)_3$ (spectrum 2) and Tb^{3+}-$(AACl)_3$ (spectrum 3). [Experimental conditions: concentration of ligand and complexes were 1×10^{-5} mol. L^{-1}, solvent = ethanol].

Upon addition of Sm(III) ions, a slight blue shift and enhancement of the absorbance value due to complex formation, (spectrum 2). A similar behavior was also observed in case of Tb^{3+} ions (spectrum 3). Moreover, the estimated ε values for the $Sm(AA)_3$ and $Tb(AA)_3$ complexes amount, respectively to 31,600 and 34,000 $mol.^{-1}$ $L\,cm^{-1}$ with a noticeable increase compared to free ligand. Compared to AA ligand and their Tb(III) or Sm(III) complexes, the monitored UV absorption spectra of ligand AACl (λ_{max} 348 nm, ε = 30,760 $mol.^{-1}$ $L\,cm^{-1}$), their Tb(III) and Sm(III) counterparts (Fig. 1B) indicate increased blue shift by 4–7 nm and higher estimated ε values 38200 and 42,000 $mol.^{-1}$ $L\,cm^{-1}$, respectively. These results reflect and further confirm the role of Cl atom in reinforcing lanthanoid-AACl coordination through two oxygens of carboxylate group rather than the preferential O- and N-coordination sites elucidated in lanthanoid-AA complexation.

Biological activity

The antibacterial activity of the parent ligands and their metal complexes against *A. flavus* and *Canidia albicans* fungi, *S. aureus* (G+) and *E. coli* (G−) bacteria was tested in order to assess their potential antimicrobial effects [35–37]. The biological activity of the ligands and their metal complexes were also compared with *tetracycline* (Antibacterial agent) and *Amphotericin B* (Antifungal agent). Such organisms can achieve resistance to antibiotics through biochemical and morphological modification [27]. In the present work all the synthesized complexes gave no inhibition zone diameters values towards *A. flavus* fungus. The two ligands AA, AACl and their complexes showed a considerable biological activity towards *S. aureus* (G+) and *E. coli* (G−) bacteria with inhibition zone diameters ranging from 10 to 17 mm/mg sample (Fig. 2). The ligands and their complexes gave inhibition zone diameters values ranging from 10 to 12 mm/mg sample towards *C. albicans* fungus with the exception of $Tb(AA)_3$ which showed no biological activity towards this type of fungi [38]. Most of the reported complexes showed enhanced biological activity towards *S. aureus* (G+), *E. coli* (G−) bacteria and *C. albicans* fungus with respect to that of the free ligands AA and AACl. These results mean that, the activity of the studied ligands against different microorganisms is generally enhanced by chelation with the biologically active metal. This would suggest that chelation could facilitate the ability of such complexes to cross a cell membrane and can be explained by Tweedy's Chelation Theory [39]. On chelation, the delocalization of π-electrons over the whole chelate ring will be increased and that enhance the penetration of the complexes into lipid membranes and blocking the metal binding sites in the enzymes of microorganisms. Furthermore, AACl and their Sm(III) and Tb(III) showed relatively higher biological activity than AA and Ln-$(AA)_3$ counterparts. This refers to a role of Cl atom in increasing the biological activity. Also, the tested complexes may disturb the respiration process of the cell and consequently block the synthesis of proteins leading to no further growth of the organisms [40]. The variation in the activity values of different compounds against different organisms depends on either the impermeability of the cells of the microbes or on the differences in ribosome of microbial cells [41].

Molecular orbital calculations

From the elemental analysis and spectroscopic data, Sm(III) and Tb(III) ions were expected to be coordinated to AA ions through a nitrogen atom of NH_2 group and oxygen of the carboxylate group forming the six membered ring complexes. On the other hand, Sm(III) and Tb(III) ions were bonded to AACl ion through only the two oxygen of the carboxylate ion forming four membered ring complexes. In this section, we try to study the ground state geometry of the two ligands AA and AACl and their complexes with Sm(III) and Tb(III) ions and to explain why AA bonded through N10 and O8-atoms, and AACl bonded through O8 and O9-atoms.

Geometry and ground state of ligands

The optimized structure of the two ligands AA and AACl are depicted in Fig. 3 with numbering of the atoms. The energies of the ground state computed by B3LYP/6-311++G^{**} are presented in Tables 4 and 5. In addition, the computed parameters were compared with the corresponding values obtained from the experimental data. The optimized bond length of C—C in phenyl ring falls in the range from 1.393 to 1.428 Å which are in good agreement with those of experimentally reported values (c.f. Table 4). The optimized C2—Cl11 bond length obtained by B3LYP/6-311++G^{**} is 1.741 Å which is also in good agreement with the experimental value 1.744 Å [42]. For the C—O bonds, the optimized length is slightly shorter than the experimental values (c.f. Table 4). The bond angles for DFT – B3LYP/6-311++G^{**} reported in Table 4 are slightly better than the HF-method compared to experimental results. The computations overestimate the <HNH and <OCO

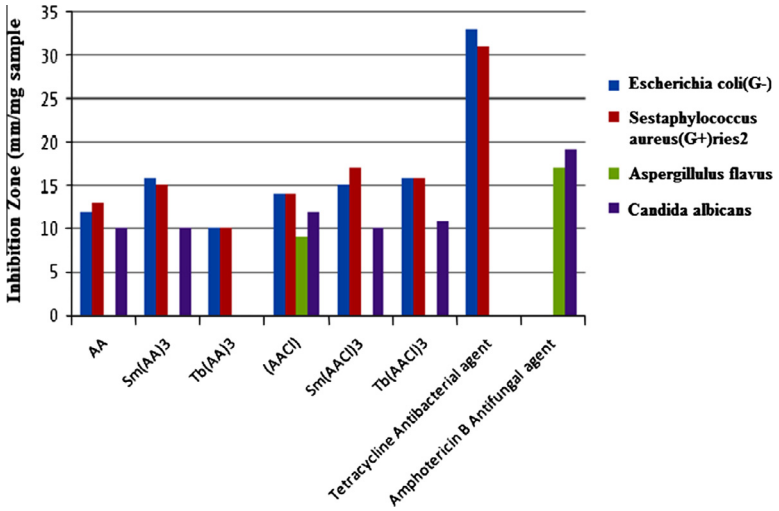

Fig. 2. Antimicrobial activity of AA and AACl ligands and their samarium and terbium complexes.

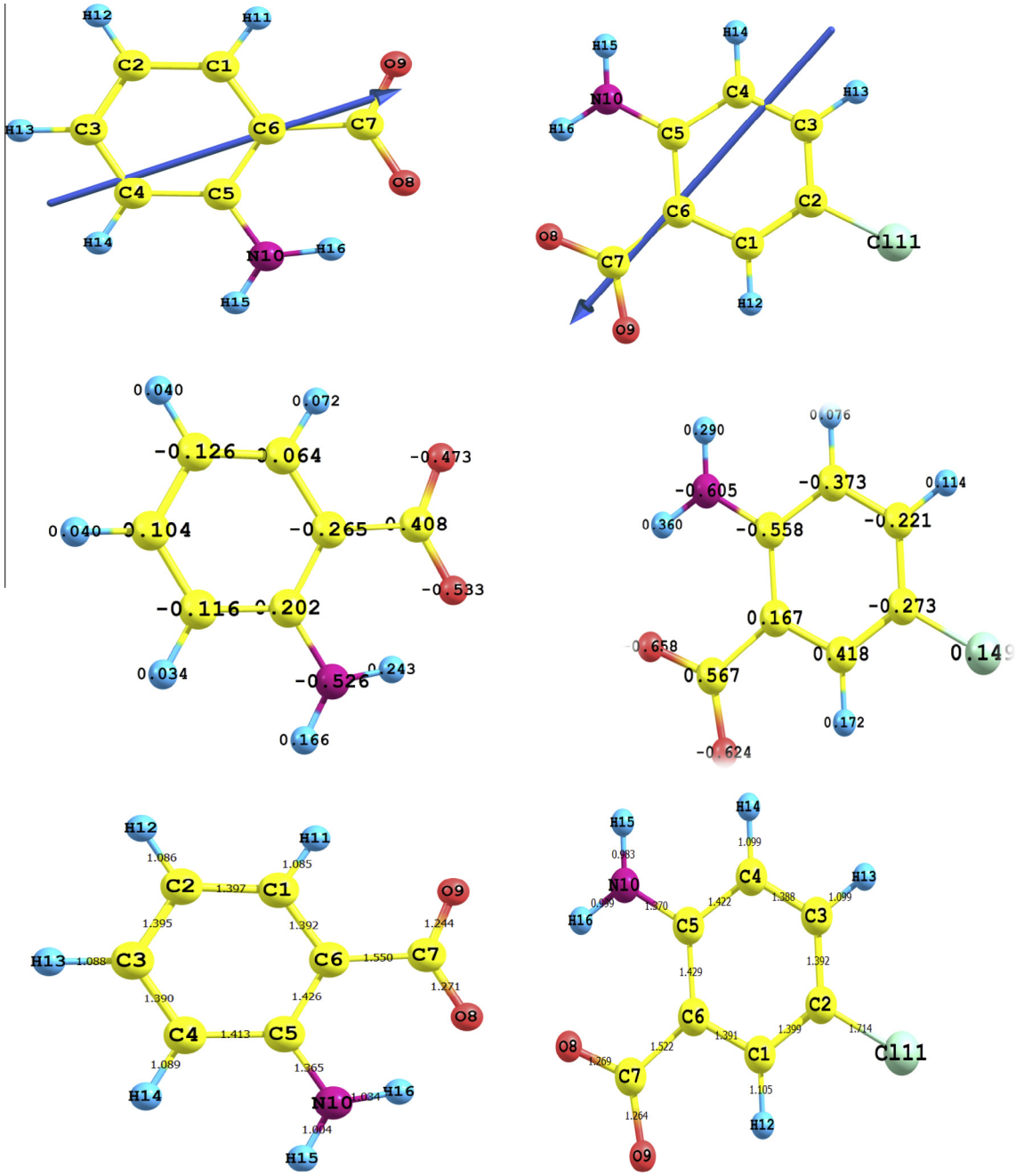

Fig. 3. Optimized geometry, vector of dipole moment, numbering system, net charges and HOMO and LUMO charge density maps for AA and AACl ligands using B3LYP/6-311G**.

angles. From the analysis of geometric parameters; we notice such differences between calculated and measured values. These discrepancies can be explained by the fact that the calculations assume an isolated molecule where the intermolecular columbic interactions with the neighboring molecules are absent, whereas the experimental results correspond to interact molecules in the crystal lattice for a similar compound.

The ligand AA is considered as electron donor, whereas, ligand AACl is electron acceptor as indicated from the E_{HOMO} and E_{LUMO} (c.f. Table 5). The ligand AA is more reactive than AACl as reflected from energy gap values (c.f. Table 5). From the computed net charge on active centers, it was found that the most negative centers in AA are N10 and O8. Whereas in ligand AACl, the most negative centers are O8 and O9. The reason why AA ligand bonded through N10 and O8 while AACl ligand bonded through O8 and O9-atoms. The computed dipole moment of AA ligand is 8.38D. Insertion of Cl-atom in C5-atom as in AACl increases the dipole moment to 10.19D indicating that the vector of the dipole moment of Cl-atom is in the same direction of the vector of AA-ligand.

Geometric parameters of the complexes

Tables 6–9 in addition to Fig. 4 present the optimized geometry, numbering system, the vector of the dipole moment, the energetic, dipole moment, energy gap, energy of HOMO and LUMO, net charge on active centers, bond lengths, bond angles and dihedral angles of all metal complexes studied in this work. In the complexes of $Sm(AA)_3$ and $Tb(AA)_3$ the metal ion coordinates with N10, O12, N27, O26 and N42, O39 to form six-member ring.

Table 4
Bond lengths, Bond angles and dihydral angles for AA and AACl using B3LYP/6-311++G**.

Parameter	AA	AACl	Expt[57]
Bond length, Å			
C1—C2	1.399	1.399	1.374
C1—C6	1.398	1.391	1.403
C2—C3	1.401	1.392	1.385
C3—C4	1.393	1.388	1.366
C4—C5	1.415	1.422	1.411
C5—C6	1.428	1.429	1.411
C6—C7	1.546	1.522	1.464
C7—O8	1.277	1.269	1.320
C7—O9	1.252	1.264	1.229
C5—N10	1.369	1.370	1.364
N10—H15	1.006	0.983	0.879
N10—H16	1.031	0.999	0.879
C2—Cl11	–	1.714	1.744
Bond angle, degree			
<C1 C6 C5	118.1	1119.0	119.67
<C1 C2 C5	118.6	120.4	121.6
<C2 C3 C4	120.2	119.5	120.9
<C3 C4 C5	121.1	121.0	121.6
<C4 C5 C6	118.9	118.6	117.3
<C5 N10 H16	114.1	118.8	118.5
<C1 C6 C7	118.8	117.1	121.5
<O8 C7 O9	126.8	122.3	121.4
<H15 N10 H16	124.9	121.3	119.1
<C1 C2 Cl11	–	120.0	

Table 5
Total energy, energy of HOMO and LUMO, energy gap and dipole moment for AA and AACl using B3LYP/6-311++G**.

Parameter	AA B3LYP/6-31++G**	AACl B3LYP/6-31++G**
E_T, au	−475.6737	−935.2676
E_{HOMO}, au	−0.06282	−0.6454
E_{LUMO}, au	0.08358	0.07876
E_g, eV	3.98	19.68
μ, D	8.39	10.19

Table 6
Total energy, energy of HOMO and, LUMO, energy gap and dipole moment for the studied complexes using SDDALL.

Parameter	Sm(AA) O—N	Tb(AA) O—N	Sm(AACl) O—O	Tb(AACl) O—O
E_T, au	−905.6308	−1070.4615	−947.9705	−1113.142
E_{HOMO}, au	−0.35752	−0.34257	−0.31084	−0.30478
	−0.35751		−0.31082	
E_{LUMO}, au	0.04446	0.04504	0.04397	0.04493
	0.04454		0.04399	
Eg, eV	10.93	10.54	9.65	9.51
μ, D	19.13	9.70	13.03	12.97

In complexes of $Sm(AACl)_3$ and $Tb(AACl)_3$, the metal ion coordinates with O14, O15, O27, O28 and O40, O44 to form four member ring. The geometric changes that are observed in the ligand moiety itself are insignificant except C (phenyl) with NH_2 and COOH groups show shortness upon complexation with the metal ion. The bonds between M and the ligand sites in $M(AA)_3$ complexes i.e. M—N and M—O are too long, 2.730 Å for M—N10, 2.758 Å for M—N27, 2.728 Å for M—N42, 2.160 Å for M—O12, 2.182 Å for M—O26 and 2.171 Å for M—O39 compared to the typical M—N and M—O bonds [43]. The too long M—N bonds for $M(AA)_3$ complexes mean that the ionic character of these bonds is small. In case of $M(AACl)_3$, the M—O bonds is of the same range of the typical M—O bonds [44]. This means that, the ionic character in case of $M(AACl)_3$ complexes is greater than the $M(AA)_3$ complexes. Also, the charge on the metal ion in the complex is much less than 3, hence, the comparison between the calculated (B3LYP/6-311++G**) and the typical M(III)—N and M(III)—O is not very precise. The calculated values of the bond angles (between metal ion and binding sites) < MNC and <OMN, in case of $M(AA)_3$ vary between 61° and 124° which compare nicely with the experimental data obtained from X-ray data for O_h complexes indicates octahedral geometry [45]. In case of $M(AACl)_3$ complexes, the <OMO, <MOC and <OCO angles vary between 55° and 95° which compare with the experimental data reported in literature [46]. The values of the dihedral angles around metal ion (c.f. Tables 7 and 8) in $M(AA)_3$ complexes, are far from 0.0° or 180° which indicate that the metal ion is not in the same plane of the donating sites. On the other hand, the dihedral angles of the $M(AACl)_3$ complexes (c.f. Tables 7 and 8) are 0.0° and 180° indicating that the metal ion is in the same molecular plane of the donating sites.

All the studied complexes are polar compounds as it is evident from the magnitude of their dipole moment (c.f. Table 6). As the energy gap of the studied complexes decreases, the reactivity of the complexes increases. In our complexes, the reactivity follows the order $Tb(AACl)_3 > Sm(AACl)_3 > Tb(AA)_3 > Sm(AA)_3$. The complexes of $M(AACl)_3$ are donor complexes than $M(AA)_3$ complexes as reflected from its ionization energy (c.f. Table 6).

Charge distribution analysis

Table 9 presents the net charge on active centers of the studied metal complexes and the amount of charge transferred from the ligands to the central metal ions, i.e. $(AA)_3 \rightarrow M$ and $(AACl)_3 \rightarrow M$. The results of Table 9 show that $Sm(AA)_3$ metal ion received 1.116 e, $Tb(AA)_3$ metal ion received 1.227e, $Sm(AACl)_3$ metal ion received 1.599e and $Tb(AACl)_3$ received 1.592e from its surrounding ligands. Also from the results of Table 9, there is a large electron back-donation from the metal ion to the donating sites N10, O12, N27, O26, N42 and O39 in (AA) and O14, O15, O27, O28, O40 and O41 in (AACl). These results are further confirmed by comparing the values of the calculated charge on the liganding atoms in the complexes and on the same atoms in the free ligand. In the all studied complexes, the charge density increases on the donating atoms after complexation.

Structure activity relationship

The biological activity of the prepared complexes can be correlated to the calculated geometrical parameters and ground state properties. From Fig. 2 and Tables 5, 6 and 9 one can reveal the following:

- The higher reactivity of $Sm(AACl)_3$ and $Tb(AACl)_3$ complexes over $Sm(AA)_3$ and $Tb(AA)_3$ can be explained in terms of the energy gap which measure the reactivity, as the energy gap decreases the reactivity increases, and the amount of electronic charge transfer from the ligand to the central metal ion increases.
- Theoretically, the reactivity of the prepared complexes follows the order: $Tb(AACl)_3 > Sm(AACl)_3 > Tb(AA)_3 > Sm(AA)_3$ which is of the same order of the reactivity towards G− and G+ (c.f. Fig. 2).
- The Mullikan electronic charge from the ligand to the central metal ion of the studied complexes follows the order: $Sm(AACl)_3 > Tb(AACl)_3 > Tb(AA)_3 > Sm(AA)_3$ which is of the same order of the reactivity towards G− and G+ (c.f. Fig. 2).

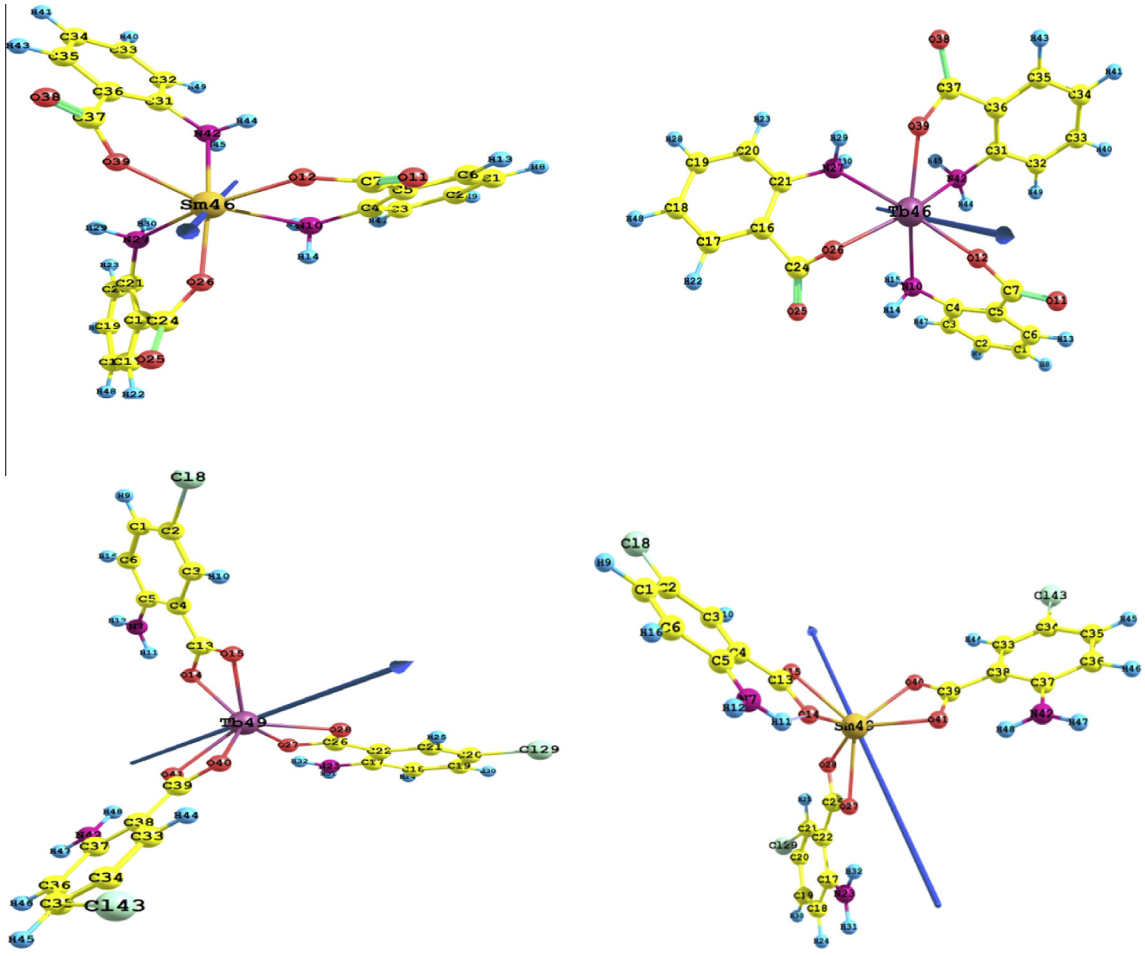

Fig. 4. Final geometry, numbering system and vector of The dipole moment for metals complexes using SDDALL.

Table 7
Bond lengths, bond angles and dihydral angles for the metal-AA complexes using SDDLL.

Parameter	AA		Parameter	AA	
	Sm	Tb		Sm	Tb
M—N10	2.730	2.614	C24—O25	1.214	1.233
M—O12	2.160	2.128	C37—O38	1.208	1.222
M—N27	2.758	2.789	<O12 M N10	68.8	70.1
M—O26	2.182	2.183	<O26MN27	65.7	67.0
M—O39	2.171	2.158	<O39 M N42	64.5	61.6
M—N42	2.728	2.569	<M N42 C31	124.1	115.6
C31—N42	1.460	1.459	<N42 C31 C36	125.8	122.2
C13—C36	1.397	1.401	<C31 C36 C37	115.6	122.8
C36—C37	1.504	1.499	<C36 C37 O39	−157.8	114.5
C37—O39	1.306	1.312	<M N10 C4 C3	54.7	−163.7
O12—C7	1.314	1.306	<M O12 C7 C5	58.7	−62.4
C5—C7	1.500	1.513	<M O26 C24 C16	58.2	−86.7
C4—C5	1.409	1.407	<M N27 C21 C20	−160.6	161.8
C4—N10	1.453	1.464	<M O39 C37 C36	57.3	−6.3
C21—N27	1.454	1.455	<M N42 C31 C32	−167.1	131.1
C16—C21	1.396	1.395			
C16—C24	1.502	1.489			
C24—O26	1.308	1.304			
C7—O11	1.225	1.225			

Table 8
Bond lengths, bond angles and dihydral angles for the metal-AACl complexes using SDDLL.

Parameter	AA-Cl		Parameter	AA-Cl	
	Sm	Tb		Sm	Tb
M—O14	2.377	2.357	<M O15 C13 C4	179.0	179.7
M—O15	2.381	2.327	<O15 C13 C4 C3	0.11	0.44
M—O27	2.405	2.364	<M O28 C26 C22	−179.9	−179.9
M—O28	2.359	2.320	<O28 C26 C22 C21	−0.3	0.11
M—O40	2.355	2.326	<M O40 C39 C38	−179.7	−179.5
M—O41	2.398	2.357	<O40 C34 C38 C33	0.384	−0.11
C4—C13	1.448	1.446			
C22—C26	1.448	1.446			
C38—C39	1.450	1.447			
C2—Cl 8	1.829	1.830			
C20—Cl 29	1.829	1.830			
C24—Cl 43	1.830	1.830			
<O14 M O15	54.8	55.5			
<M O14 C13	27.5	27.8			
<O14 C13 O15	116.4	115.3			
<M O15 C13	94.3	95.3			
<O27 M O28	54.7	55.5			
<O40 M O41	63.5	62.9			

Table 9
Net charges on metals and active centers of the studied complexes.

Center AACl	AA		Center	AA CI	
	Sm	Tb		Sm	Tb
M	1.884	1.773	M	1.401	1.408
N10	−0.933	−0.951	O14	−0.784	−0.769
O12	−0.971	−0.900	O15	−0.689	−0.677
O11	−0.525	−0.514	O27	−0.777	−0.776
O26	−0.980	−0.884	O28	−0.690	−0.670
N27	−0.912	−0.916	O40	−0.691	−0.678
O25	−0.513	−0.563	O41	−0.779	−0.774
N42	−0.923	−0.948	N7	−0.864	−0.870
O39	−0.967	−0.988	N23	−0.866	−0.894
O38	−0.502	−0.525	N42	−0.870	−0.868
$(AA)_3 \rightarrow M$	1.116	1.227	$(AACl)_3 \rightarrow M$	1.599	1.592

Conclusions

Four solid lanthanide complexes of Sm(III) and Tb(III) with Antharnilic acid (AA) and chloroanthanilic acid (AACl) were prepared and isolated. According to elemental analysis, IR, mass spectroscopy, and thermal analyses, these complexes are structurally formulated in 1:3 [Metal]:[Ligand] ratio. From the IR spectra, it is clear that the active site in AA is O8 and N10 but in AACl is O8 and O9. Therefore, a chlorine-affected coordination and reactivity-diversity was emphasized. The complexes have not water molecules inside or outside the coordination sphere of the central metal according to thermal analysis. The theoretical calculations of the ligand and their complexes show a difference in the geometric parameters between calculated and experimental results. These discrepancies can be explained by the fact that the calculations assume an isolated molecule where the intermolecular columbic interaction with the neighboring molecules are absent, whereas the experimental results corresponds to interacting molecules in the crystal lattice for a similar compound. Also the calculation shows that, the ligand AA is considered as electron donor and more reactive than ligand AACl. Insertion of chlorine atom as in AACl ligand increases the value of the dipole moment. The values of the dihedral angles around metal ion in $M(AA)_3$ complexes are far from 0.0° or 180° which indicate that the metal ion is not in the same plane of the donating sites. On the other hand, the dihedral angles of the $M(AACl)_3$ complexes are 0.0° and 180° indicating that the metal ion is in the same molecular plane of the donating sites. All the studied complexes are polar as it is evident from the magnitude of their dipole moment. The reactivity of the complexes follows the order $Tb(AACl)_3 > Sm(AACl)_3 > Tb(AA)_3 > Sm(AA)_3$. Most of the reported complexes showed enhanced biological activity towards *S. aureus* (G+) and *E. coli* (G−) bacteria and *C. albicans* fungus with respect to that of the free ligands AA and AACl.

References

[1] P. Wiklund, J. Bergman, Curr. Org. Chem. 3 (2006) 379–402.
[2] H. Stepan, E. Staudacher, Anal. Biochem. 418 (2011) 24–29.
[3] I. Sosič, S. Turk, M. Sinreih, N. Trošt, O. Verlaine, A. Amoroso, A. Zervosen, A. Luxen, B. Joris, S. Gobec, Acta Chim. Slov. 59 (2012) 380–388.
[4] B. Goel, T. Ram, R. Tyagi, E. Bansal, A. Kumar, D. Mukherjee, J.N. Sinha, Eur. J. Med. Chem. 34 (1999) 265–269.
[5] S. Sharma, V.K. Srivastava, A. Kumar, Eur. J. Med. Chem. 37 (2002) 689–697.
[6] Y. Sarrafi, M. Mohadeszadeh, K. Alimohammadi, Chin. Chem. Lett. 20 (2009) 784–788.
[7] A.M. Farag, S.G. Teoh, H. Osman, C.S. Yeap, H.K. Fun, Acta Cryst. E67 (2011) o37.
[8] Z. Aiqin, P. Qiliang, J. Husheng, L. Xuguang, X. Bingshe, J. Rare Earth 30 (2012) 10–16.
[9] V.F. Shul'gin, S.V. Abkhairova, O.V. Konnik, S.B. Meshkova, Z.M. Topilova, E.B. Rusanov, G.G. Aleksandrov, I.L. Eremenko, Russ. J. Inorg. Chem. 58 (6) (2013) 678–683.
[10] N.P. Kuzmina, S.V. Eliseeva, Russ. J. Inorg. Chem. 51 (2006) 73–88.
[11] V.F. Shul'gin, S.V. Abkhairova, O.V. Konnik, S.B. Meshkova, Z.M. Topilova, M.A. Kiskin, I.L. Eremenko, J. Inorg. Chem. 57 (2012) 420–426.
[12] V.F. Shul'gin, O.V. Konnik, S.V. Abkhairova, A.N. Gusev, S.B. Meshkova, A.V. Kiriyak, E.B. Rusanov, M. Hasegawa, W. Linert, Inorg. Chim. Acta 402 (2013) 33–38.
[13] J.P. Leonard, C.B. Nolan, F. Stomeo, T.H. Gunnlaugsson, Top. Curr. Chem. 281 (2007) 1–43.
[14] K. Binnemans, in: K.A. Gschneidner Jr., J.C.G. Bünzli, V.K. Pecharsky (Eds.), Rare-Earth Beta-Diketonates, Handbook on the Physics and Chemistry of Rare Earth, Elsevier, Amsterdam, 2005, pp. 107–272.
[15] S.V. Eliseeva, J.C.G. Bünzli, Chem. Soc. Rev. 39 (2010) 189–227.
[16] P.C.R. Soares-Santos, R.A. Sá Ferreira, T. Trindade, L.D. Carlos, H.I.S. Nogueira, J. Alloys Compd. 451 (2008) 575–577.
[17] M. Hilder, M. Lezhnina, M.L. Cole, C.M. Forsyth, P.C. Junk, U.H. Kynast, J. Photochem. Photobiol. A 217 (2011) 76–86.
[18] M. Forsyth, K. Wilson, T. Behrsing, C. Forsyth, G.B. Deacon, A. Phanasgoankar, Corrosion 58 (2002) 953–960.
[19] Y. Kim, S.S. Yun, Thermochim. Acta 59 (1982) 299–303.
[20] G.B. Deacon, M. Forsyth, P.C. Junk, S.G. Leary, G.J. Moxey, Polyhedron 25 (223) (2006) 379–386.
[21] M. Shakiv, Y. Azim, H.T.N. Chishti, S. Parveen, Spectrochim. Acta A 65 (2006) 490–496.
[22] N. Sari, S. Arslan, E. Logoglu, I. Sakiyan, J. Anim. Sci. 16 (2003) 283–288.
[23] G.G. Mohamed, Spectrochim. Acta A 64 (2006) 188–195.
[24] (a) A.D. Becke, J. Chem. Phys. 98 (1993) 5648–5652;
(b) A.D. Becke, J. Chem. Phys. 98 (1993) 1372–1377.
[25] (a) C. Lee, W. Yang, R.G. Parr, Phys. Rev. B Condens. Matter. 37 (1988) 785–789;
(b) B. Miehlich, A. Savin, H. Stolt, H. Preuss, Chem. Phys. Lett. 157 (1989) 200–206.
[26] B.B. Stefanov, G. Liu, A. Liashenko, P. Piskorz, I. Komaromi, R.L. Martin, D.J. Fox, T. Keith, M.A. Al-Laham, C.Y. Peng, A. Nanayakkara, M. Challacombe, P.M.W. Gill, B. Johnson, W. Chen, M.W. Wong, C. Gonzalez, J.A. Pople, Gaussian, Inc., Pittsburgh PA. 2003.
[27] M.J. Frisch, G.W. Trucks, H.B. Schlegel, G.E. Scuseria, et al., Gaussian, Inc., Wallingford CT, 2009.
[28] W. Brzyska, Z. Rzaczynska, Monatsh. Chem. 119 (1988) 147–156.
[29] G.J. Efremova, R.T. Butshkova, Koord Khim. 3 (1977) 1184–1189.
[30] V.L. Dorofeev, Chem. Acta 38 (2004) 45–49.
[31] G.G. Mohamed, A.A. Soliman, Thermochim. Acta 421 (2004) 151–159.
[32] A.G. Hill, C. Curran, J. Phys. Chem. 64 (1960) 1519–1522.
[33] S.S. Sandhu, B.S. Manhas, R.M. Mittal, S.S. Parmar, Indian J. Chem. 7 (1969) 286–289.
[34] A.A. Soliman, G.G. Mohamed, Spectrochim. Acta A 91 (2012) 11–17.
[35] Z.L. You, H.L. Zhu, W.S. Liu, Z. Anorg, Allg. Chem. 630 (2004) 1617–1622.
[36] S. Yamada, Coord. Chem. Rev. 190 (1999) 537–555.
[37] S. Chang, L. Jones, C.M. Wang, L.M. Henling, R.H. Grubbs, Organometallics 17 (1998) 3460–3465.
[38] S. Duraiswamy, R.E. Michael, Z. Matthias, N. Karup-pannan, Polyhedron 26 (2007) 4314–4320.
[39] N. Dharmaraj, P. Viswanathamurthi, K. Nataragan, Transition Met. Chem. 26 (2001) 105–109.
[40] P.G. Lawrence, P.L. Harold, O.G. Francis, Antibiot. Chemother. 5 (1980) 1597–1600.
[41] A.C. Dros, R.W.J. Zijlstra, P.T. Van Duijmen, A.L. Spek, H. Kooijman, R.M. Kellogg, Tetrahedron Lett. 54 (1998) 77–87.
[42] H. Takagawa, S. Ohba, Y. Saito, Acta Cryst. C42 (1986) 1880–1881.
[43] L. Armelao, S. Quici, F. Brigelletti, G. Accorsi, G. Bottaroi, M. Cavazzini, E. Tendello, Coord. Chem. Rev. 254 (2010) 487–505.
[44] S. Tanase, J. Reedijk, Coord. Chem. Rev. 250 (2006) 2501–2510.
[45] S.S. Zumdahl, Chemistry for Chemical and Biological Science, University Science Books, USA, 2000.
[46] A.I. Boldyrev, V.V. Zhdankin, J. Simons, P.J. Stang, J. Am. Chem. Soc. 114 (1992) 10569–10572.